

Kinetic Particle Simulations of Plasma Charging and Dust Transport near Uneven Lunar Surface Terrain

Jianxun Zhao*, Guirong Yan[†], Xiaoming He[‡], and Daoru Han[§] Missouri University of Science and Technology, Rolla, Missouri 65409

This paper presents a kinetic particle simulation study of the plasma charging and dust transport near the uneven lunar surface terrain. A fully-kinetic 3-D finite-difference (FD) particle-in-cell (PIC) code is utilized to simulate the plasma interaction with uneven surface terrain. The levitation and transport of charged dust grains under the effect of the local photoelectron sheath will be investigated. The profile of quantities of interests, such as electric potential, electric field, solar wind and photoelectron density, and the concentration of charged dust within the photoelectron sheath will be presented.

I. Nomenclature

e = elementary charge

E = electric field

F = cumulative density function

m = mass

n = density

J = current density

k = Boltzmann constant

T = temperature

v = velocity

Greek letters

 ϕ = electric potential

 ε = relative permittivity

Subscript

d = drifting

f = free

m = minimum

s = surface

th = thermal

phe = photoelectron

swe = solar wind electron

swi = solar wind ion

II. Introduction

THE lunar surface is directly exposed to the solar radiation and solar wind plasma due to the lack of protection of the global atmosphere and magnetic field. The interaction between the lunar surface and the charged particles leads to

^{*}Graduate Research Assistant, Department of Mechanical and Aerospace Engineering, 400 W. 13th St., Rolla, MO 65409, AIAA Student Member.

[†]Associate Professor, Department of Civil, Architectural and Environmental Engineering. 1401 N. Pine St., Rolla, MO 65409.

[‡]Associate Professor, Department of Mathematics and Statistics. 400 W. 12th St., Rolla, MO 65409.

[§]Assistant Professor, Department of Mechanical and Aerospace Engineering, 400 W. 13th St., Rolla, MO 65409, AIAA Senior Member. handao@mst.edu

a charging process on the lunar surface, causing a negative or positive surface electric potential with respect to the ambient environment. The charging process on the lunar surface has been studied extensively [1–15]. In this paper, we study the local 3-D structure of the photoelectron sheath and its effects on the charged dust grains. The objective of this study is to investigate the electric environment inside the photoelectron sheath by simulating the interactions between charged particles and the lunar surface. A fully-kinetic 3-D finite-difference (FD) particle-in-cell (PIC) code, [7, 16], which has been validated by comparing the 1-D numerical results with solutions to semi-analytic models, is utilized to simulate the plasma interaction near the lunar surface. Dynamics of charged dust grains will be resolved in the local electrostatic environment obtained by FD-PIC simulations.

The rest of this paper is organized as follows. Section III will describe the problem and introduce the setup of the simulation. Section IV will investigate the transport dynamics of the levitated charged lunar dust grains. Section V will present results of local 3-D electrostatic plasma environment and the dust environment. Conclusions will be given in Section VI.

III. 3-D Simulations for Uneven Lunar Surface Terrain

We have presented the studies of 1-D and 2-D configurations for even and uneven lunar surface terrains in our previous work [16–18]. In this section, we will analyze the 3-D structure of the photoelectron sheath above the uneven lunar surface. The computation domain is presented in Fig.1. A cubic obstacle will be located on the ground in the center of the computation domain, representing a lunar surface construction. The solar wind enters the computation domain from the top boundary with a certain Sun elevation angle (SEA), α . The charged particles will deposit on the bottom surface of the computation domain (which is considered as the lunar surface) and the obstacle surfaces, creating a surface potential. The surface potential, together with the density above the lunar surface, controls the electric environment inside the photoelectron sheath.

A. Problem Description and Simulation Setup

In this study, we consider a 3-D computation domain with a rectangular obstacle (representing a lunar surface construction) locating on the ground surface, as shown in Fig. 1(a). An FD-PIC numerical simulation will be run to obtain the quantities of interest (electric potential, electric field, charge density, etc.) in the computation domain. Then four cases with different dust generation locations (location 1, 2, 3, and 4 in Fig. 2, which is the top view of the computation domain) will be simulated.

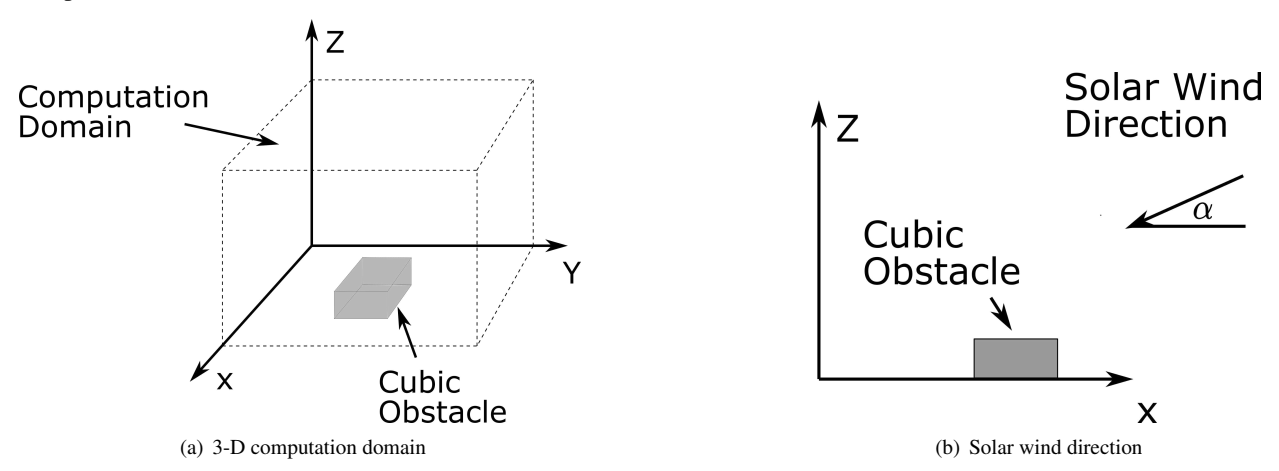


Fig. 1 Computation domain

As shown in Fig. 2, In case 1, dust are originated in front of the obstacle. Whereas in case 2, dust are disturbed in the shadow region behind the obstacle. In case 3, dust are levitated behind the shadow region of the obstacle, And in case 4, dust are generated alongside the obstacle.

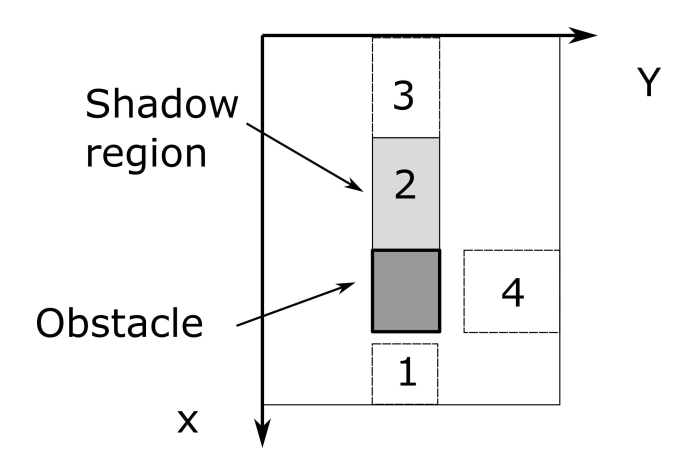


Fig. 2 Dust generation locations in different cases

B. Modeling Plasma Environment

The details of the photoelectron sheath were introduced and studied in our previous research [16, 17, 19]. In this study, we focused on the plasma and dust environment near the lunar terminator region, therefore a 10° SEA was applied in the numerical simulations.

1. Plasma Conditions and Normalization

In this study, the solar wind electrons, solar wind ions, and photoelectrons are considered as the plasma species within the photoelectron sheath. The solar wind is assumed traveling to the lunar surface with a 10° SEA and 468 km/s velocity. The solar wind electrons are considered as thermal with a temperature of 12 eV, whereas the solar wind ions are considered as cold (temperature of 0 eV). The solar wind number density is 8.7 cm⁻³. The temperature of photoelectron is 2.2 eV, and the density of photoelectron on the lunar surface is controlled by the SEA. The parameters of solar wind and photoelectrons are listed in Table 1 [7, 16, 19].

Table 1 Solar wind and photoelectron parameters (where α is the Sun elevation angle)

	Solar wind electrons	Solar wind ions	Photoelectrons
Drifting Velocity, km/s	468	468	=
Density, cm ⁻³	8.7	8.7	64 $\sin(\alpha)$
Temperature, eV	12	0	2.2
Sun Elevation Angle, °	10	10	10

In the numerical simulations, the solar wind are traveling into the computation domain through the X-Y plane. along -z-direction. At the beginning of the simulation, $\sim 1,800,000$ solar wind electrons and ions were preloaded inside the computation domain. Another $\sim 10,000$ solar wind electrons, solar wind ions, and photoelectrons are injected into the computation domain in each time step. The simulation runs 50,000 steps for each case, which is ~ 250 seconds in reality, and ~ 50 hours in wall clock time.

To increase the efficiency and reduce the complexity of numerical computation, All parameters are normalized by the references listed in Table 2 in this study, where λ_d is the Debye length of photoelectron at 90° SEA; $T_{\rm phe}$ is the photoelectron temperature; $m_{\rm phe}$ is the mass of photoelectron; k is the Boltzmann constant; e is electric charge; $v_{\rm phe,t} = \sqrt{kT_{\rm phe}/m_{\rm phe}}$ is the reference for velocity; and $n_{\rm phe,ref}$ is the photoelectron number density at 90° SEA. The PIC time is normalized by $1/\omega_{\rm phe}$, where $\omega_{\rm phe}$ is the plasma frequency of the photoelectron at normal incidence condition (90°).

Table 2 Normalization references

L_{ref}	$T_{\rm ref}$	$m_{\rm ref}$	$\phi_{ m ref}$	$v_{\rm ref}$	$n_{\rm ref}$	$t_{\rm ref}$
λ_d	$T_{\rm phe}$	$m_{ m phe}$	$\frac{kT_{\rm phe}}{e}$	$v_{\mathrm{phe,t}}$	$n_{\mathrm{phe,ref}}$	$\frac{1}{\omega_{\rm phe}}$

2. Computation Domain and Boundary Conditions

Computation Domain The configuration of the computation domain is shown in Fig. 3. The dimension of the computation domain is $70\times25\times50$ total PIC cells (physical dimension of $96.6\times34.5\times69.0$ m). A cubic obstacle which is considered as a lunar construction with a dimension of $5\times5\times5$ PIC cells (physical dimension of $6.9\times6.9\times6.9$ m) is located on the lunar surface with a shadow region behind.

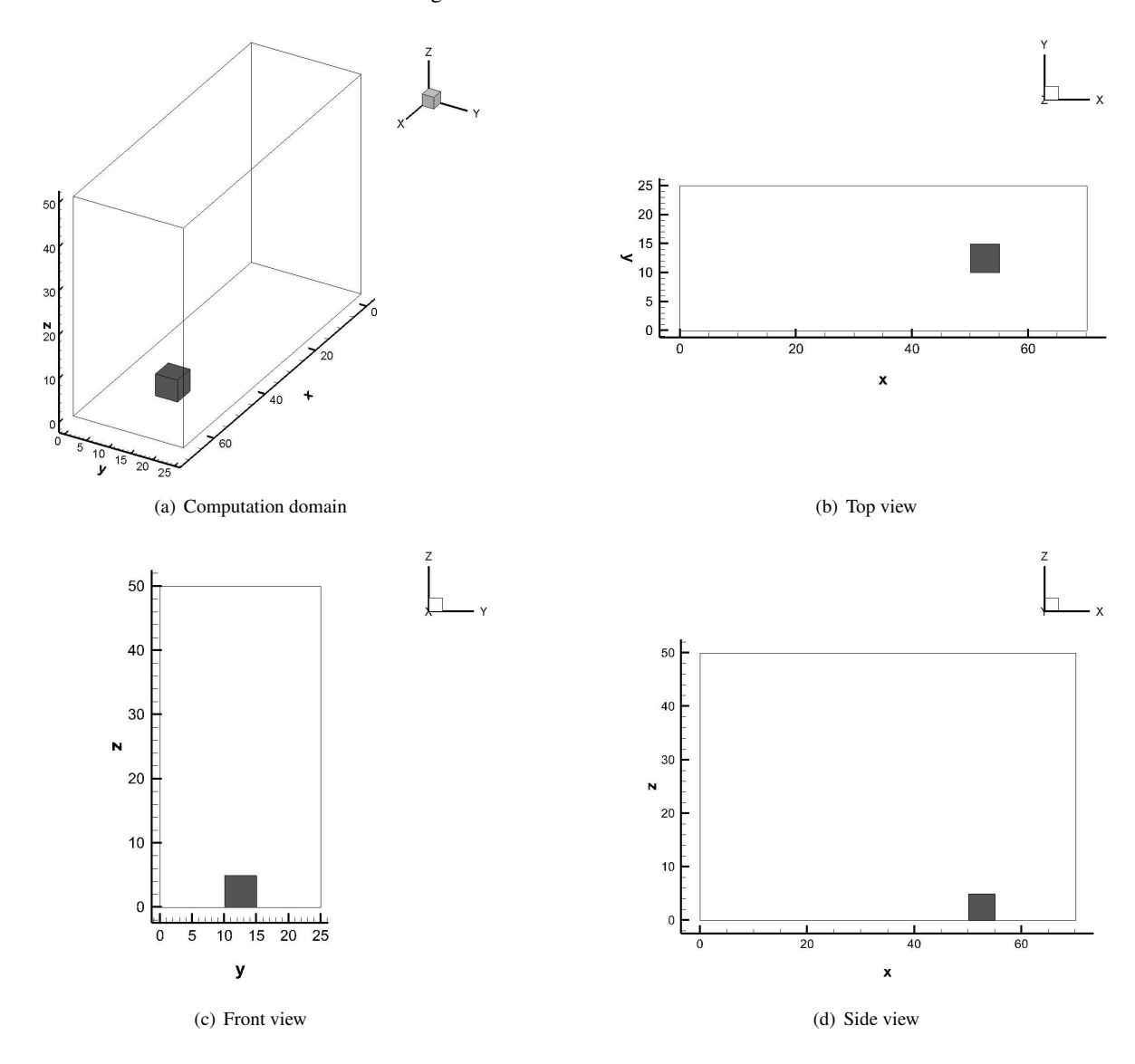


Fig. 3 Computation domain in simulation

Table 3 Boundary conditions of the computation domain

Surrounding BC	Bottom BC	Top BC
periodic	absorb	inject

Particle Boundary Conditions The boundary condition for surrounding boundaries is set as "periodic", meaning that once a particle crosses one of these boundaries. it will enter the computation domain from the opposite boundary with the same properties, therefore the computation domain represents a relatively larger domain with low computation cost in simulation. The bottom surface is set as "absorb", meaning the particle will deposit and the charge will be accumulated on the surface once it hits the surface. The top surface is set as "inject", from where the solar wind enters the computation domain. The parameters of the computation domain are listed in Table 3.

Field Boundary Conditions The zero-Dirichlet boundary condition where $\phi = 0$ is applied for the Z_{max} boundary, where is considered as infinity in the numerical simulation. All other boundaries are applied with the zero-Neumann boundary condition where $\frac{\partial \phi}{\partial n} = 0$.

IV. Transport of Levitated Dust Grains

A. Generation of Lofted Charged Dust Grains

In this study, the dust grains are assumed to be originated from the lunar surface with a slightly upward velocity, simulating lifted dust grains disturbed by human or mechanical activities on the lunar surface. In total four dust generation areas are considered in the numerical simulation, as introduced in Section III.A and Fig. 2.

B. Transport of Charged Dust Grains

To simplify the numerical model, all dust grains are considered as spheres with radius r_d . The dust grain dynamics follows Newton's second law as shown in Eq. (1).

$$\mathbf{F} = m_d \frac{\mathrm{d}\mathbf{v}}{\mathrm{d}t} = Q_d \overrightarrow{\mathbf{E}}(\overrightarrow{z}) - m_d g \tag{1}$$

where m_d and Q_d are the mass and charge of the dust grain, respectively; \mathbf{v} is the velocity vector; \mathbf{E} is the electric field vector, which is obtained from the FD-PIC simulation; and g is the lunar gravitational acceleration. It should be noted that the last term on the right hand side of Eq. (1), $m_d g$, only applies for z vector.

A simplified charge models which were introduced in [7] are utilized to calculate Q_d in numerical simulations, as shown in Eq. (2). In the numerical model, the charge on each dust grain is assumed to be large enough to activate an electrostatic levitation, hence all dust grains are guaranteed to be lofted from the surface.

$$Q_d = (1 + \delta)Q_{d,min} \tag{2}$$

where $Q_{d,min} = (m_d g)/E_s$, E_s is the electric field along z axis on the lunar surface (i.e., $E_s = E_z(z=0)$); $\delta \ll 1$ gives an initial acceleration to dust grains ($\delta = 0.05$ is assumed in this study).

According to Eqs. (1) and (2), the equations of motion of dust grains within photoelectron sheath can be obtained as Eq. (3).

$$\frac{d^2x}{dt^2} = \left[(1+\delta) \frac{E_x(x,y,z)}{E_s} \right] g$$

$$\frac{d^2y}{dt^2} = \left[(1+\delta) \frac{E_y(x,y,z)}{E_s} \right] g$$

$$\frac{d^2z}{dt^2} = \left[(1+\delta) \frac{E_z(x,y,z)}{E_s} - 1 \right] g$$
(3)

where E_x , E_y , and E_z are the electric field along x, y, and z, respectively.

V. Results of plasma environment and dust transport

A. Plasma Environment

The details of the 2-D photoelectron sheath structure has been studied in our previous research [17], here we will introduce the 3-D plasma environment in the photoelectron sheath.

The distributions of potential and total density within the photoelectron sheath are shown in Figs. 4 and 5. The density of each species is shown in Fig. 6.

As seen in Fig. 4(a), a nearly neutral potential profile can be observed in most areas above the lunar surface, due to the density neutrality in these areas (see Fig. 5(a)). The emission of photoelectrons caused by the exposure to sun light, leads to a positive potential on the front and top surfaces of the obstacle and the lunar surface outside the shadow region. Whereas the lack of sun light leads to a negative potential inside the shadow region.

It is reasonable that the potential is much higher near the front surface of the obstacle, due to the larger photoelectron density (caused by the relatively greater incidence angle on the front surface) and the corresponding larger amount of positive charges accumulated on the front surface.

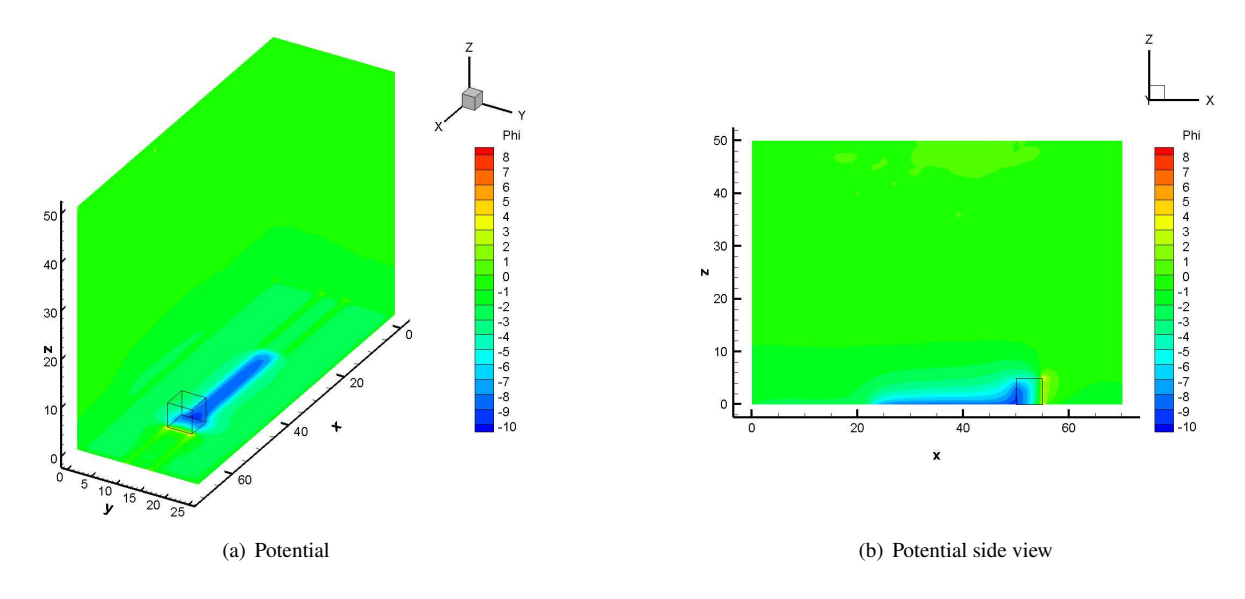


Fig. 4 Electric potential, normalized by 2.2 V

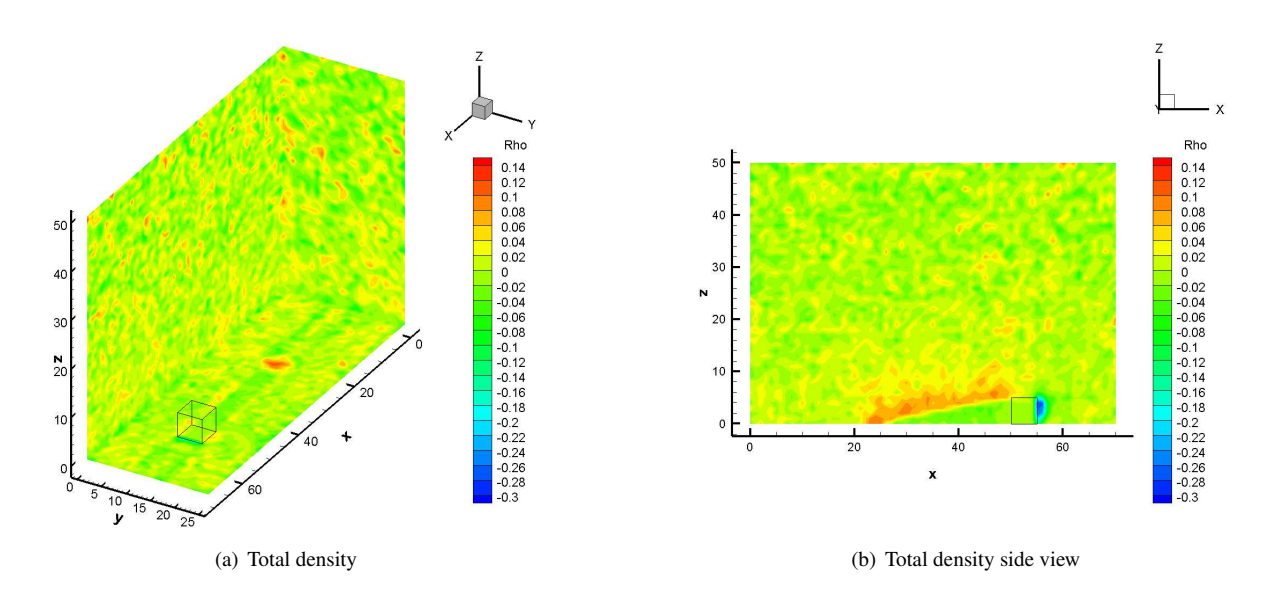


Fig. 5 Total density, normalized by 64 cm⁻³

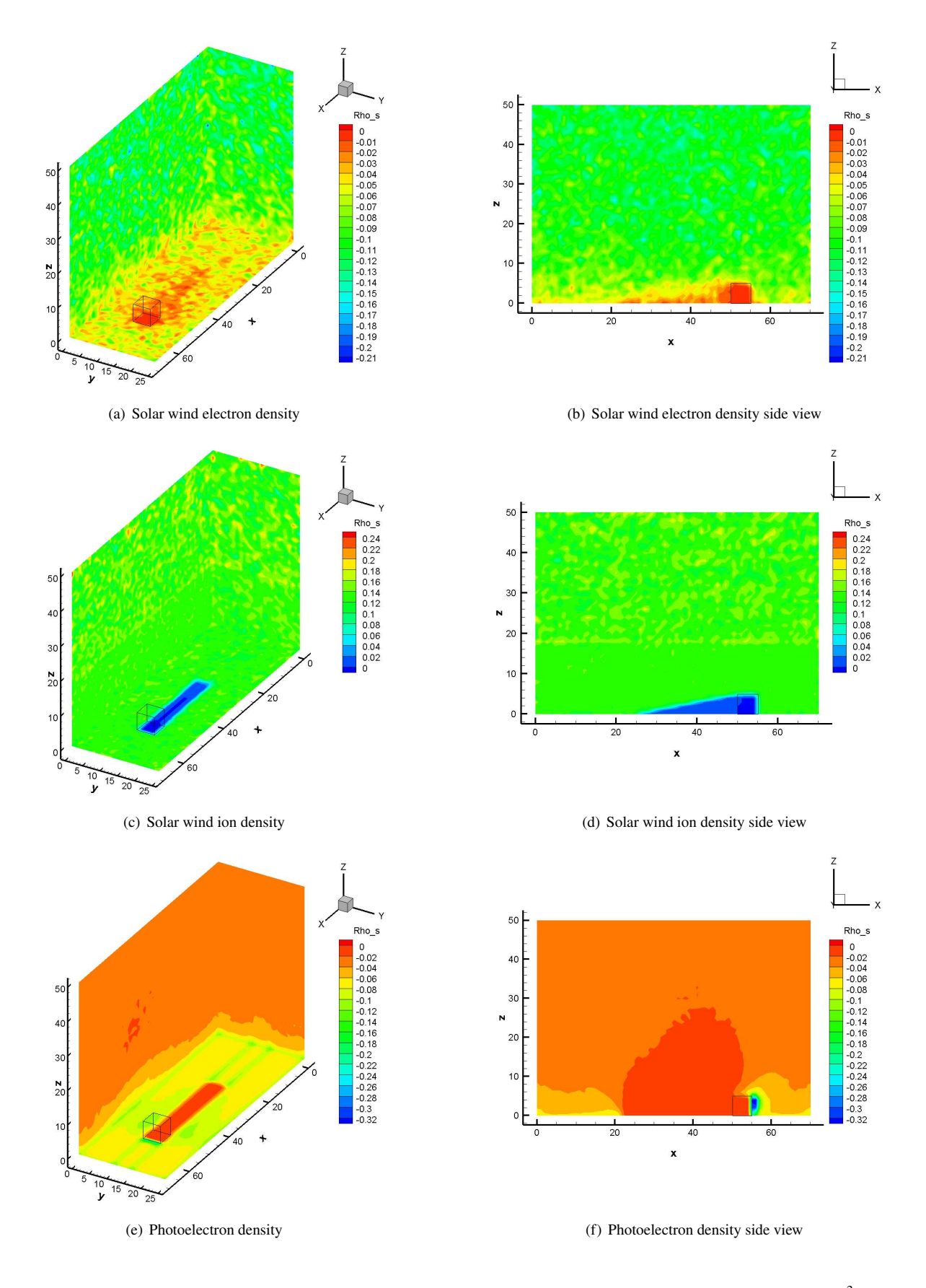


Fig. 6 Density of solar wind electrons, solar wind ions, and photoelectrons, normalized by 64 cm⁻³

B. Dust Environment

As introduced in Section IV.B, all dust grains are considered as spheres with same radius $(1.0 \times 10^{-6} \text{ m})$ in this study. The motion of the dust are controlled by the governing equations introduced in Section IV.B. Since the physical initial dust density that originated from the lunar surface is random and can be affected by a number of conditions (concentration of dust grains on the lunar surface, strength of human activities, etc.) The initial non-dimensional dust density is set as 1.0 for each case in the simulation to present the ratios of dust density at different locations compared with the initial disturbed and levitated dust grains. The concentration of dust grains in the computation domain that generated at different locations are presented below.

1. Case 1

The concentration of dust grains that originated in front of the obstacle (Case 1) is shown in Fig. 7. With a radius of 1.0×10^{-6} m and initial upward velocity of 0.1 m/s, most of the dust will be levitated and concentrated within ~ 2 m from the lunar surface under 10° SEA in the average solar wind condition. However, a slight amount of dust can be lofted much higher (upto ~ 60 m) and distributed inside the entire computation domain, due to the greater accumulated electric charge and the corresponding greater electrostatic force acting on the dust (see Fig. 7(b)).

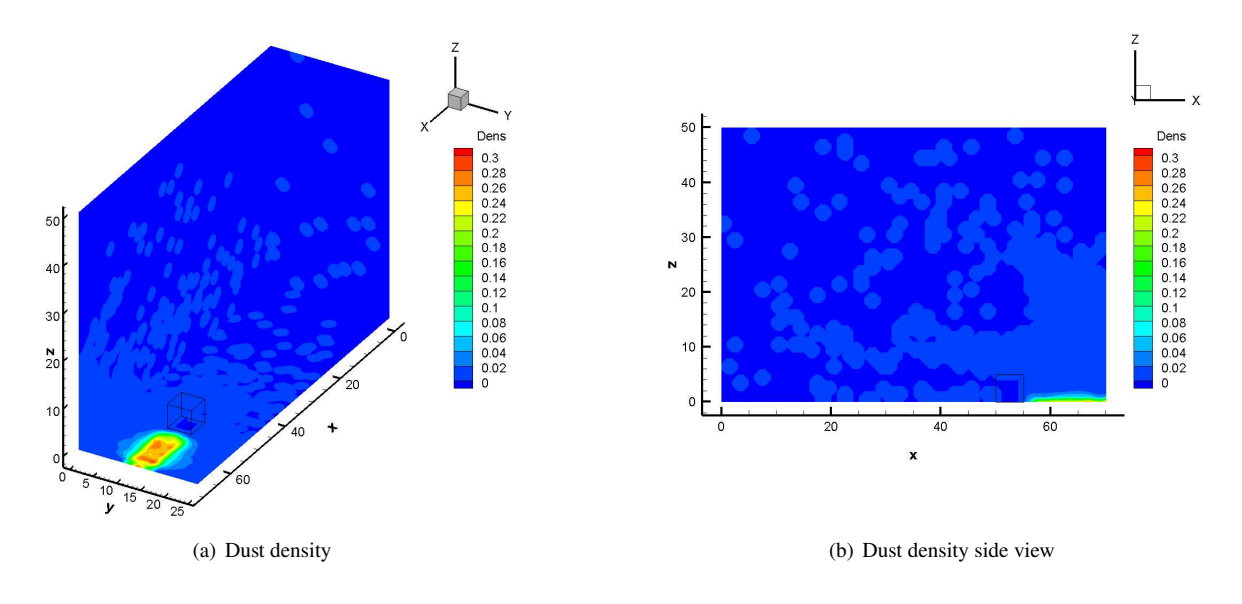


Fig. 7 Dust density of Case 1

2. Case 2

Slightly different from Case 1, The dust lofted in Case 2 are not distributed into a large area. The dust grains generated inside the shadow region are concentrated within ~ 2 m height from the lunar surface. The levitation height is slightly higher for the dust that closer to the obstacle. A slight amount of dust can be lofted to ~ 13 m above the surface behind the obstacle. It can be seen that some dust are able to reach as high as ~ 55 m right above the top of the obstacle.

3. Case 3

Similar to Case 1, the levitation height of the dust grains originated behind the shadow region of the obstacle is ~ 2 m from the lunar surface. A slight amount of dust can be distributed in a larger area around the origination of the dust. It can be seen in Fig. 9(b) that the charged dust in Case 3 can be distributed into the shadow region behind the obstacle, whereas these dust will not distribute within a certain height (~ 41 m) above and in front of the obstacle.

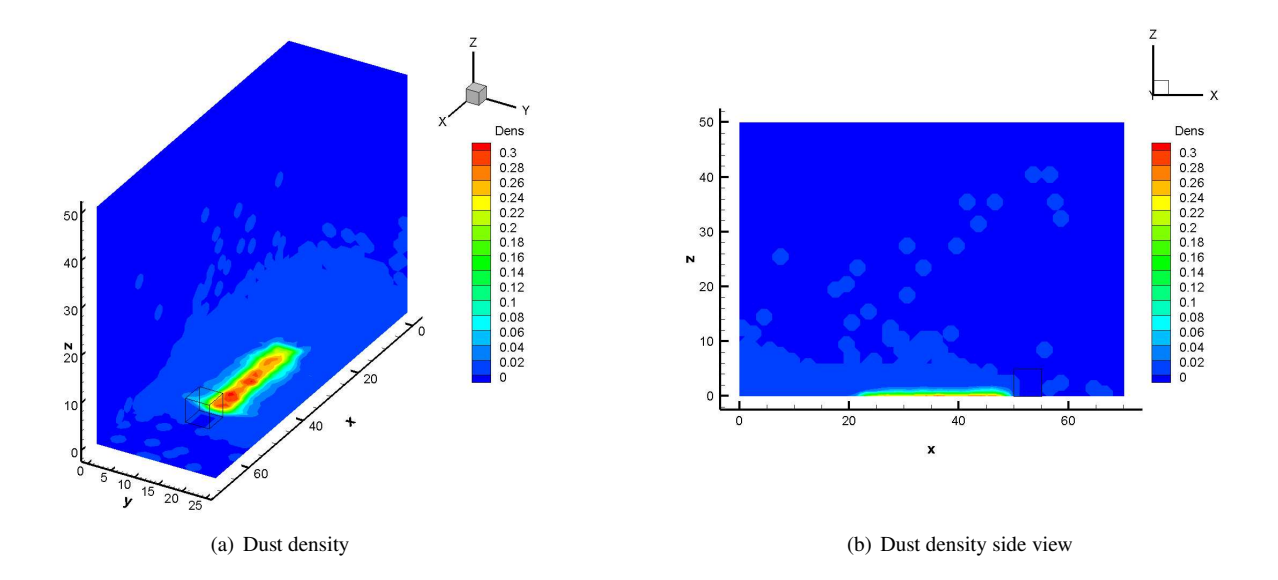


Fig. 8 Dust density of Case 2

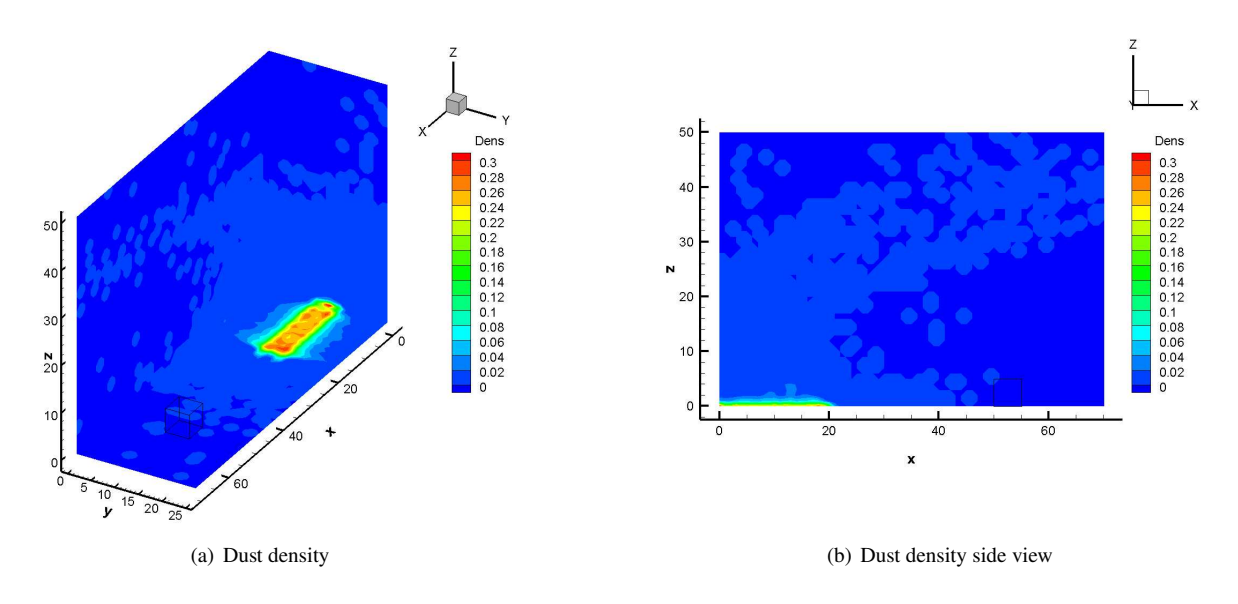


Fig. 9 Dust density of Case 3

4. Case 4

In Case 4, the dust grains originated alongside the obstacle will still concentrate within ~ 2 m from the lunar surface. The further from the obstacle, the greater the density and lofted height of the dust will be (see Fig. 10(a)). A slight amount of dust can be levitated to as high as the top surface of the obstacle. It can be seen from Fig. 10(b) that some of the dust can reach to ~ 50 m. This can be caused by a greater accumulated electric charge on the dust, however it is not a general situation for charged dust grains, because only several dust grains can reach such a height in Fig. 10(b).

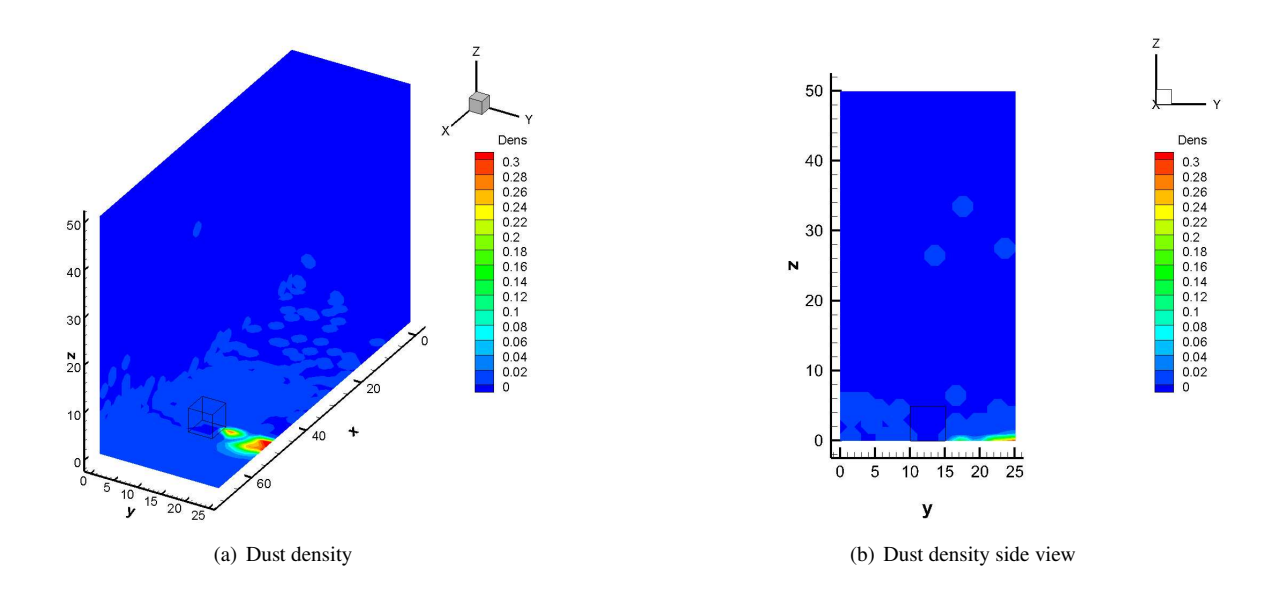


Fig. 10 Dust density of Case 4

VI. Conclusion

In this study, we presented the 3-D photoelectron structure at lunar terminator region (with 10° SEA) with a cubic obstacle representing lunar surface construction in the computation domain. The quantities of interests within the photoelectron sheath (electric potential, charge density, electric field, etc.) were obtained with FD-PIC simulation. We also presented the 3-D dust concentration of the lofted charged lunar dust that originated from different locations inside the computation domain.

The numerical results showed that with a 10° SEA under average solar wind condition, the lunar surface potential can reach from -22 V in the shadow region behind the construction to ~ 20 V on the front surface of the construction. With a initial upward velocity of 0.1 m/s, most of the charged lunar dust that originated from different locations will concentrate within a region of ~ 2 m height from the lunar surface. A slight amount of dust with greater accumulated charge can be levitated higher and distributed into a larger area. The highest height that the dust originated alongside the construction can reach is lower compared with the dust originated from other locations.

The ongoing work is to extend our work to cover a larger range of SEA, and multiple charge models to calculate the accumulated charge on each dust grain. We will also upgrade the FD-PIC code to simulate the two-way coupled interaction between electrostatic field and the charged lunar dust grains.

Acknowledgments

This work was partially supported by NASA-Missouri Space Grant Consortium through NASA-EPSCoR-Missouri, as well as NSF through grants DMS-2111039 and CBET-2132655. The simulations presented here were performed with computing resources provided by the Center for High Performance Computing Research at Missouri University of Science and Technology through an NSF grant (OAC-1919789).

References

- [1] Fu, J. H. M., "Surface potential of a photoemitting plate," Journal of Geophysical Research, Vol. 76, No. 10, 1971, pp. 2506-2509. doi:10.1029/JA076i010p02506, URL https://agupubs.onlinelibrary.wiley.com/doi/abs/10.1029/JA076i010p02506.
- [2] Willis, R., Anderegg, M., Feuerbacher, B., and Fitton, B., "Photoemission and Secondary Electron Emission from Lunar Surface Material," *Photon and Particle Interactions with Surfaces in Space*, Astrophysics and Space Science Library, Vol. 37, edited by R. Grard, Springer Netherlands, 1973, pp. 389–401. doi:10.1007/978-94-010-2647-5_25, URL http://dx.doi.org/10.1007/978-94-010-2647-5_25.
- [3] Zook, H. A., and McCoy, J. E., "Large scale lunar horizon glow and a high altitude lunar dust exosphere," *Geophysical Research Letters*, Vol. 18, No. 11, 1991, pp. 2117–2120. doi:10.1029/91GL02235, URL http://dx.doi.org/10.1029/91GL02235.
- [4] Nitter, T., Havnes, O., and Melandsø, F., "Levitation and dynamics of charged dust in the photoelectron sheath above surfaces in space," *Journal of Geophysical Research: Space Physics*, Vol. 103, No. A4, 1998, pp. 6605–6620. doi:10.1029/97JA03523, URL http://onlinelibrary.wiley.com/doi/10.1029/97JA03523/abstract.
- [5] Abbas, M., Tankosic, D., Craven, P., Spann, J., LeClair, A., and West, E., "Lunar dust charging by photoelectric emissions," *Planetary and Space Science*, Vol. 55, No. 7-8, 2007, pp. 953–965. doi:10.1016/j.pss.2006.12.007, URL http://www.sciencedirect.com/science/article/pii/S003206330600359X.
- [6] Halekas, J. S., Delory, G. T., Brain, D. A., Lin, R. P., Fillingim, M. O., Lee, C. O., Mewaldt, R. A., Stubbs, T. J., Farrell, W. M., and Hudson, M. K., "Extreme lunar surface charging during solar energetic particle events," *Geophysical Research Letters*, Vol. 34, No. 2, 2007, p. L02111. doi:10.1029/2006GL028517, URL http://onlinelibrary.wiley.com/doi/10.1029/2006GL028517/full.
- [7] Wang, J., He, X., and Cao, Y., "Modeling Electrostatic Levitation of Dust Particles on Lunar Surface," *IEEE Transactions on Plasma Science*, Vol. 36, No. 5, 2008, pp. 2459–2466. doi:10.1109/TPS.2008.2003016.
- [8] Poppe, A., and Horányi, M., "Simulations of the photoelectron sheath and dust levitation on the lunar surface," *Journal of Geophysical Research*, Vol. 115, No. A8, 2010, p. A08106. doi:10.1029/2010JA015286.
- [9] Poppe, A., Halekas, J. S., and Horányi, M., "Negative potentials above the day-side lunar surface in the terrestrial plasma sheet: Evidence of non-monotonic potentials," *Geophysical Research Letters*, Vol. 38, No. 2, 2011, p. L02103. doi:10.1029/2010GL046119, URL http://onlinelibrary.wiley.com/doi/10.1029/2010GL046119/abstract, space Sciences.

- [10] Poppe, A. R., "Modeling, Theoretical and Observational Studies of the Lunar Photoelectron Sheath," Ph.D. thesis, University of Colorado, Boulder, 2011.
- [11] Halekas, J. S., Delory, G. T., Farrell, W. M., Angelopoulos, V., McFadden, J. P., Bonnell, J. W., Fillingim, M. O., and Plaschke, F., "First remote measurements of lunar surface charging from ARTEMIS: Evidence for nonmonotonic sheath potentials above the dayside surface," *Journal of Geophysical Research*, Vol. 116, No. A7, 2011, p. A07103. doi:10.1029/2011JA016542, URL http://onlinelibrary.wiley.com/doi/10.1029/2011JA016542/abstract, solar and Heliospheric Physics.
- [12] Poppe, A. R., Piquette, M., Likhanskii, A., and Horányi, M., "The effect of surface topography on the lunar photoelectron sheath and electrostatic dust transport," *Icarus*, Vol. 221, 2012, pp. 135–146.
- [13] Stubbs, T., Farrell, W., Halekas, J., Burchill, J., Collier, M., Zimmerman, M., Vondrak, R., Delory, G., and Pfaff, R., "Dependence of lunar surface charging on solar wind plasma conditions and solar irradiation," *Planetary and Space Science*, Vol. 90, 2014, pp. 10–27. doi:10.1016/j.pss.2013.07.008, URL https://www.sciencedirect.com/science/article/pii/S0032063313001876.
- [14] Wang, X., Schwan, J., Hsu, H.-W., Grün, E., and Horányi, M., "Dust charging and transport on airless planetary bodies," *Geophysical Research Letters*, Vol. 43, No. 12, 2016, pp. 6103–6110. doi:10.1002/2016GL069491, URL http://onlinelibrary.wiley.com/doi/10.1002/2016GL069491/full.
- [15] Zimmerman, M. I., Farrell, W. M., Hartzell, C. M., Wang, X., Horanyi, M., Hurley, D. M., and Hibbitts, K., "Grain-scale supercharging and breakdown on airless regoliths," *Journal of Geophysical Research: Planets*, Vol. 121, No. 10, 2016, pp. 2150–2165. doi:10.1002/2016JE005049, URL http://onlinelibrary.wiley.com/doi/10.1002/2016JE005049/abstract.
- [16] Zhao, J., Wei, X., Hu, Z., He, X., Han, D., Hu, Z., and Du, X., "Photoelectron Sheath near the Lunar Surface: Fully Kinetic Modeling and Uncertainty Quantification Analysis," AIAA Scitech 2020 Forum, 2020. doi:10.2514/6.2020-1548, URL https://arc.aiaa.org/doi/abs/10.2514/6.2020-1548.
- [17] Zhao, J., Wei, X., He, X., Han, D., and Du, X., "Fully-Kinetic Particle-in-Cell Simulations of Photoelectron Sheath and Dust Levitation on Uneven Lunar Surface," AIAA Scitech 2021 Forum, 2021. doi:10.2514/6.2021-1433, URL https://arc.aiaa.org/doi/abs/10.2514/6.2021-1433.
- [18] Zhao, J., Wei, X., Du, X., He, X., and Han, D., "Photoelectron Sheath and Plasma Charging on the Lunar Surface: Semianalytic Solutions and Fully-Kinetic Particle-in-Cell Simulations," *IEEE Transactions on Plasma Science*, Vol. 49, No. 10, 2021, pp. 3036–3050. doi:10.1109/TPS.2021.3110946.
- [19] Lund, D., Zhao, J., Lamb, A., and Han, D., "Fully Kinetic PIFE-PIC Simulations of Plasma Charging at Lunar Craters," AIAA Scitech 2020 Forum, 2020. doi:10.2514/6.2020-1549, URL https://arc.aiaa.org/doi/abs/10.2514/6.2020-1549.